On the development and validation of FAGE for local measurement of tropospheric OH and HO2

On the Development and Validation of FAGE for Local Measurement of Tropospheric OH and HO_2

M. R. Heal, D. E. Heard, M. J. Pilling, and B. J. Whitaker

School of Chemistry, University of Leeds, Leeds, United Kingdom

ABSTRACT

A fluorescence assay by gas expansion (FAGE) instrument based on laser-induced fluorescence designed both for laboratory validation studies and for field measurements of OH and HO_2 is described. Laboratory validation centers around the development of techniques for assessing interference from O_3 photolysis and calibration of the OH signal. Excitation at 308 nm will be employed, reducing the extent of O_3 photolysis, together with detection of OH at high and low rotational levels. The latter technique is based on the production of rotationally excited OH in the $O(^1D)$ + H_2O reaction. Calibration is centered on discharge flow and water photolysis. Optimization of the experiment relies on detailed photochemical modeling, and the proposed techniques are discussed. Attention is also paid to the possible effects of the supersonic flow field on the fluorescence assay, and the feasibility of developing a computational fluid dynamics model is discussed.

1. Introduction

The hydroxyl radical plays an important role in the chemistry of the troposphere through its reaction with methane, CO, and other volatile organic compounds. It has a short chemical lifetime ($\sim$1 s) and a low concentration ($\sim 10^6$ cm^{-3}). Its close coupling to chemical processes occurring in the troposphere and the absence, because of its short lifetime, of significant surface sources and sinks make OH an ideal species for testing the validity of tropospheric photochemical models. The low concentrations of OH, however, make its detection particularly demanding.

Techniques based on laser-induced fluorescence (LIF) have figured strongly in attempts to monitor OH in the troposphere. Off-resonance methods were tried first, with OH being excited to $A^2\Sigma^+(v' = 1)$ at 282 nm and detected at $\sim$310 nm via the (0, 0) and (1, 1) bands (Wang et al. 1976; Davis et al. 1976; Hard et al. 1984; Hard et al. 1986). This approach led to substantial interference from photolytically generated OH from photolysis of O_3 at 282 nm (Smith and Crosley 1990). Two LIF techniques have been proposed to overcome this problem. The first involves excitation of OH ($X^2\Pi$) to $v'' = 1$ using an infrared laser at 2.8 μm, followed by excitation to $A^2\Sigma^+(v' = 0)$ at 345 nm and fluorescence detection near 310 nm (Bradshaw et al. 1984).

The second approach is based on resonant excitation and detection of OH fluorescence [$A^2\Sigma^+(v' = 0)$ $\leftrightarrow$ $X^2\Pi$ ($v'' = 0$)] coupled with the FAGE (fluorescence assay by gas expansion) technique in which the atmospheric pressure sample is expanded to a pressure of a few Torr via a nozzle (Chan et al. 1990; Stevens et al. 1994 and references therein). The reduction in pressure significantly reduces the fluorescence quenching and increases the lifetime of the $A^2\Sigma^+(v = 0)$ state to $\sim$500 ns. This increase, coupled with gating of the detector, allows the separation of fluorescence and scattered light signals; in addition, the reduced quenching results in little loss in signal, despite the reduction in the hydroxyl radical density.

In this paper, we describe plans for the construction at Leeds of a laser system based on this second approach. The project is funded by the U.K. Natural Environment Research Council (NERC). The major initial aims are the testing and validation of the technique, and the proposed approach is discussed in detail below. Plans are also being developed for field testing of the system at the Weybourne Field Station in Norfolk, United Kingdom, in late 1995, with further field campaigns planned for 1996.

The key to the development of a satisfactory and sensitive instrument is an understanding of the physicochemical processes occurring in the expansion and in the excitation and deexcitation of OH. The Leeds instrument, which is described in section 2, is specifically designed to permit probing of the structure of the expansion wave by the incorporation of a stepper motor drive allowing the nozzle to be translated along the beam axis. These measurements will be supplemented

Corresponding author address: Dr. D. E. Heard, School of Chemistry, University of Leeds, Leeds LS2 9JT, United Kingdom.
E-Mail: dwayneh@chem.leeds.ac.uk

by computational fluid dynamical calculations of the expansion to aid optimization and understanding (sections 3 and 4).

Two important experimental aspects are the minimization of interference from photolytically generated OH and the calibration of the OH signal. Section 5 discusses a technique for assessing the magnitude of the interference using coupled detection of OH in low and high rotational states. This approach is based on the generation of rotationally excited OH in the interfering $O(^1D) + H_2O$ reaction. Section 6 examines approaches to calibration based on photolytic and discharge techniques.

Finally, in section 7, the modeling of the photochemical system is discussed. Smith and Crosley (1990) stress the importance of modeling to ascertain the effects of photochemical interference, collisional energy transfer, and quenching. Our proposed approach is based on their detailed model but also employs lumping techniques that permit fewer initial assumptions to be made and employ objective methods to reduce the dimensionality of the kinetic equations. Such an approach promises to provide a technique that permits a full on-line analysis of the field data. It will be particularly valuable when coupled with concomitant measurements of other species and especially of ozone. The FAGE technique can also be used to detect HO_2 by stoichiometric conversion to OH via the reaction with NO (Hard et al. 1992a). The optimization of this technique will also be examined by modeling, and its validity will be tested in the proposed Weybourne experiments against a radical amplifier system.

2. Instrumentation

The experimental approach to FAGE follows that pioneered by other research groups in the field (Chan et al. 1990; Hofzumahaus et al. 1990; Stevens et al. 1994 and references therein; Hard et al. 1992b). The main components of the FAGE instrument being constructed at Leeds are the following: 1) a sample chamber with translatable inlet nozzle for characterization of the gas expansion, 2) a high-repetition-rate pulsed laser system, and 3) collection optics and a gated photomultiplier tube for detection of laser-induced fluorescence. These are described in turn.

a. Sampling chamber

The sample chamber, shown schematically in Fig. 1, consists of a large, vertically orientated cylindrical cell, with an internal diameter of 22 cm, mounted on a separate table from the optical bench. The excitation beam enters and exits the cell in the horizontal plane through two arms, each of length 35 cm and containing a series of variously angled baffle rings with clear aperture of 7 mm. The arms are sealed with Brewster angled quartz flats.

The air sample enters the chamber through a 1-mm diameter nozzle vertically above the beam path. The nozzle is mounted within the flexible bellows of a stepper motor driven z-shift (Creative Vacuum Technology, DZSM/150/50), which allows precise, reproducible control of the laser-probed region along the principle axis of the vertical gas beam expansion. This control over the intersection of gas beam with laser beam will enable us to fully characterize the profile of the beam expansion. The high gas throughput required to maintain the background pressure in the cell at 1 Torr or less is provided by an Edwards EH1200/E1M80 mechanical booster and rotary vacuum pump combination via an ISO 160 diameter bellows beneath the cell. The flow rate is controlled by a VAT series 12 gate valve. A pumping capability of this magnitude readily maintains the required pressure drop across the inlet hole and the linear gas velocity needed to replace the air sample at the probe region between each laser shot ($\sim$100 μs).

b. Laser system

Tunable radiation at around 308 nm is obtained using a copper vapor laser (Oxford Lasers ACL-35) pumped Lambda Physik FL3001 dye laser. The copper vapor laser, configured with unstable resonator optics to reduce beam divergence, is capable of operation at a pulse rate up to 10 kHz and will deliver an output power in excess of 35 W at its optimal operating frequency of 7 kHz. For reasons of space the two lasers are located one above the other on a double-decked table with the output beam from the copper vapor laser focused through a 1-mm pinhole and collimated to a beam radius of about 8 mm as it is folded into the dye laser. The dye solution contains a mixture of Rhodamine 6G (0.15 g l^{-1}) and Rhodamine 640 (0.12 g l^{-1}) in ethanol, chosen to maximize the output at 616 nm. This is frequency doubled using a KDP crystal, and the UV separated from the red fundamental by means of a standard assembly of four Pellin–Broca prisms. With an input power into the dye laser of 20 W, an output power of 200 mW at 308 nm, or the equivalent of 28 μJ pulse^{-1}, is routinely obtained. An intracavity airspaced etalon is available to reduce the excitation linewidth from $\sim$0.2 to $\sim$0.04 cm^{-1} in the fundamental beam (and $\sim$140% of these values in the UV). The dye laser stepper motors for grating, doubling crystal, and etalon can be computer controlled via an IEEE GPIB interface with a PC.

The pulse energy of the UV beam may be controlled by transmission of the beam through a Soleil–Babinet compensator and polarizer combination prior to entry into the sample cell. Beam-shaping and collimating optics expand the UV beam to a diameter of 5 mm.

c. Fluorescence detection

The fluorescence from the excited OH is detected mutually perpendicular to the laser beam and the gas
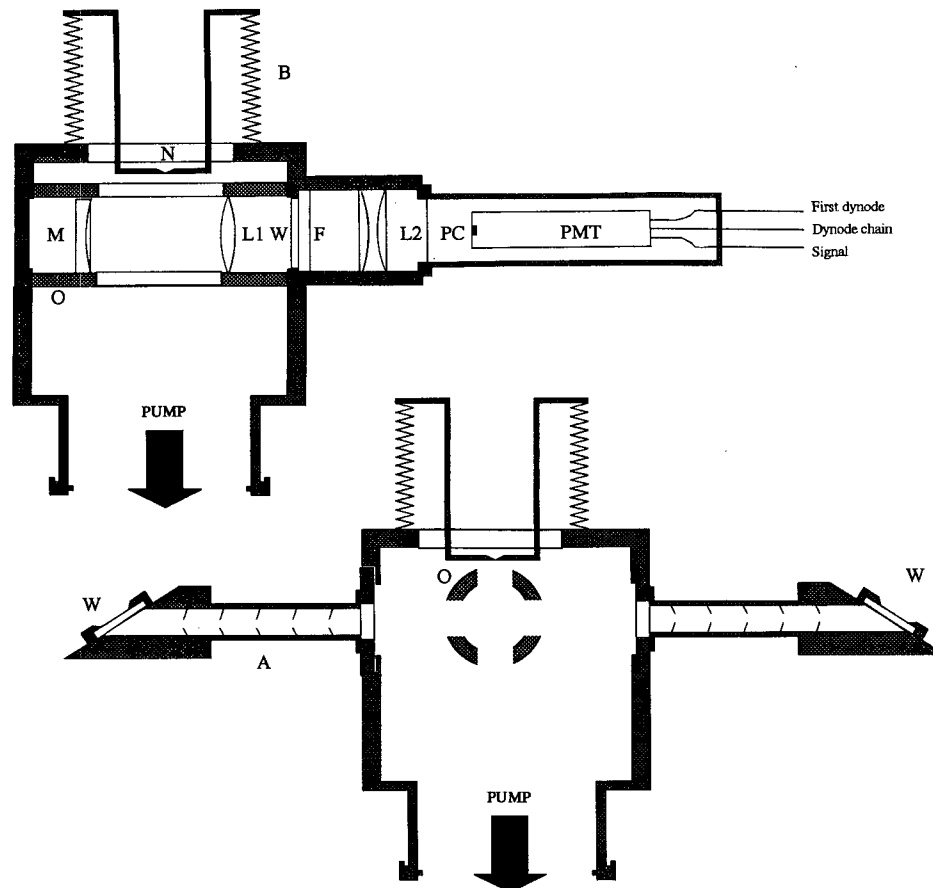
FIG. 1. Schematic diagram showing two projections of the FAGE chamber. The excitation beam enters and exits the cell in the horizontal plane through the two long arms, each of length 35 cm and containing a series of variously angled baffle rings with clear aperture of 7 mm. The fluorescent light is collected at right angles to the excitation beam by means of a f1 mirror/lens arrangement that collimates the light through a narrow bandwidth interference filter. Condensing lenses are used to focus the light onto the photocathode of a fast photomultiplier tube. Key: A—baffled arms, B—translatable bellows, F—308-nm interference filter, L1—collimating lens, L2—condensing lenses, M—concave mirror, N—nozzle, O—optical rail, PC—2.5-mm diameter photocathode, PMT—photomultiplier tube, W—fused silica window.

flow using an end-window photomultiplier (PM) tube with bialkali cathode (EMI 9893/100QB). This PM tube was specially selected for its low background count of 20 counts s^{-1}, small after-pulse signal, and the small effective photocathode diameter of 2.5 mm, which further eliminates detection of off-axis scatter. The voltage divider has been configured so that the voltage on the first dynode is independently controllable. The very high gain (8.3×10^7) and quantum efficiency (22% at 308 nm) of this PM tube were considered to outweigh the advantages of a microchannel plate detector (Stevens et al. 1994 and references therein) in respect of ease of gated operation.

A spherical mirror of 50-mm diameter and 50-mm radius of curvature (f1 optics) is mounted inside the cell along the optical axis of the PM tube as a rear reflector to double the solid angle of collected fluores-cence. Along the same axis, also inside the cell, a 50-mm focal length condenser lens collimates the fluorescence, which then passes through a quartz window, a narrowband interference filter (Acton Corporation λ_{max} = 310 nm, FWHM bandwidth = 12 nm), and is focused onto the photocathode with two plano-convex lenses. Kinematic mounts and axial adjustments ensure that the optical components are optimally configured. Individual photon signals are amplified and counted using a Stanford Research Systems SR440 300-MHz pre-amplifier and SR400 photon counter. The fluorescence signal can be normalized by monitoring the laser UV output with a separate photodiode and gated integrator (SR250) assembly.

Since the FAGE detection scheme is characterized by fluorescence on-resonance to the excitation radiation, great care is required to discriminate the weaker

fluorescence signal from the more intense background signal caused by scattering of the laser off the walls of the chamber and by Rayleigh scattering from air molecules or Mie scattering from aerosol particles. This can lead to saturation of the photocathode and spurious afterpulsing. In addition to the use of precise collection optics for spatial discrimination, the signal to noise ratio is considerably enhanced by gain switching of the photomultiplier and gating the photon counting. The voltage to the first dynode of the PM tube is switched by $\sim$400 V for the duration of the laser pulse ($\sim$20 ns) through the cell to prevent detection of secondary electrons. After switching the gain back on again, the start of photon counting is delayed further because of the RF noise induced in the electronics by the rapid switching in 40–50 ns of the first dynode voltage. In our experiments to date we find that a delay of around 200 ns relative to the start of the laser pulse is needed, but we anticipate that it will be possible to reduce this with better RF shielding of the detection chain electronics. The reduced number of molecular collisions for the excited OH in the low-pressure gas beam means that time integration over the rest of the fluorescence decay still results in capture of about 50% of the signal photons, but clearly the fluorescence lifetime τ_{fl} under the experimental conditions must be known. A second timing gate between laser shots is used to count photons for subtraction as a continuous general background.

3. The isentropic gas expansion

The viability of the FAGE technique is founded upon two ideas: First, that photochemical intcreference from O_3 photolysis in the presence of H_2O can be reduced by working at low pressures, since the reaction rate of $O(^1D)$ atoms with water will scale with the collision frequency and, second, that by reducing the pressure the radiative lifetime of the laser-excited OH radicals can be extended to close to the natural radiative lifetime, thus allowing temporal discrimination of the fluorescence from Rayleigh scattered light. To achieve this, the ambient air is expanded into a low-pressure chamber. The reduction in number density as a result of the expansion does not, however, lead to a reduction in fluorescence intensity because this effect is counterbalanced by the concomitant decrease in the electronic quenching rate (Hard et al. 1984). It is important to characterize the properties of such expansions to optimize the experimental geometry and to assess the influence of photochemical interference, particularly in polluted air samples.

Expansion of a gas into a low-pressure chamber through a nozzle whose diameter is large compared to the local mean free path of the molecules is the basis of a supersonic molecular beam (Campargue 1984; Miller 1988). For such sources (Fig. 2) the gas flow can be approximately represented as an isentropic flow (see section 4). Ambient air (pressure: P_0 and temper-
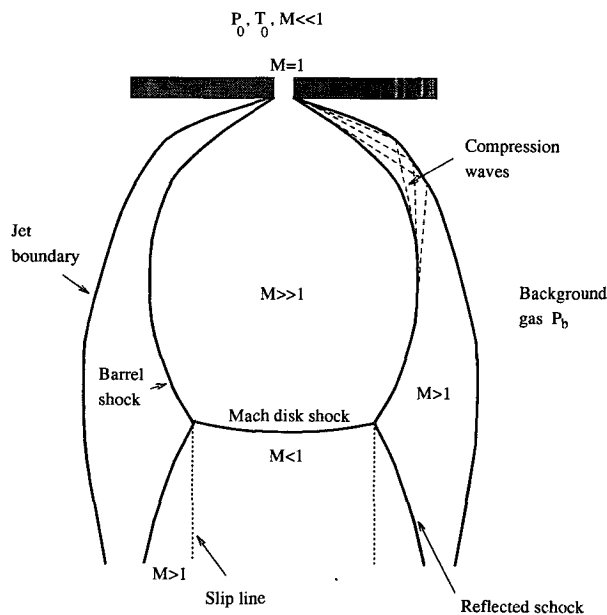

FIG. 2. The structural features of an isentropic expansion.

ature: T_0) is accelerated toward the nozzle by the pressure difference $P_0 - P_b$ between the atmosphere and the low pressure FAGE chamber. Provided that the pressure ratio P_0/P_b exceeds a critical factor, G, the gas flow reaches sonic speeds at the nozzle (Mach number $M = 1$). The parameter G, given by $((\gamma + 1)/2)^{\gamma/(\gamma-1)}$ where γ is the specific heat ratio, is less than 2.1 for all gases. Under these conditions the pressure at the exit of the nozzle is independent of P_b and equal to P_0/G, that is, approximately half the stagnation pressure. Since the pressure at the nozzle exceeds the background pressure in the chamber, the gas expands, but, for a supersonic flow ($M > 1$), the velocity _increases_ as the flow area increases. Furthermore, the fact that the gas flow is moving faster than the local speed of sound means that the expanding gas is unable to sense the boundary conditions imposed by the background gas. The result is the creation of shock waves—with large density, pressure, and temperature gradients—of thickness of the order of the local mean free path. The shock fronts "protect" the expanding core from the background gas and provide a mechanism to change the direction of the flow and eventually slow it to subsonic velocities ($M < 1$), whereupon the gas flow can adjust to the downstream boundary conditions.

The transition from supersonic to subsonic flow occurs at a downstream distance from the nozzle, x_M, which defines the centerline position of a shock structure known as the Mach disc. The position of the Mach disc turns out to be rather insensitive to the specific heat ratio γ and, measured in nozzle diameters, is given by

$$(x_M/d) = 0.67(P_0/P_b)^{1/2}. \qquad (1)$$

Essentially, this is the point at which the local gas density matches the background gas density. However, depending on the pressure ratios, a situation can arise where the compression of the expanding gas by the shock fronts causes the Mach disc to be ''underexpanded,'' and so the structure is repeated downstream. Such phenomena are seen, for example, in the plume of a high-performance jet engine and have been observed in the gas flow of a FAGE apparatus (A. Hofzumahaus 1993, personal communication). It is worth noting that the diameters of the barrel shock and Mach disc are approximately given by $\sim 0.75 x_M$ and $\sim 0.5 x_M$, respectively. Clearly the spatial extent of the laser beam at the sampling point should be closely matched to the diameter of the gas flow. Experiments by Hofzumahaus and Holland (A. Hofzumahaus 1993, personal communication) indicate that the diameter of the gas flow in their FAGE instrument is consistent with this model.

Most FAGE apparatuses are assumed to monitor the OH in the subsonic region. Given the physical dimensions ($d = 0.1$ cm) and parameters ($P_b = 1$ Torr) of a typical instrument, one expects from Eq. (1) that the position of the first Mach disc shock front should be about 1.85 cm downstream from the inlet nozzle, and since it is usual to probe some 6–10 cm downstream of the nozzle, this does not appear to be an unreasonable assumption. However, to our knowledge, this has not been verified experimentally. These are potentially important considerations, because as a result of the isentropic expansion the gas may cool considerably in the initial supersonic expansion. Assuming that the gas is predominantly nitrogen, the mean free path of molecules in the subsonic downstream region is of order 50 μm. Since $V - T$ energy transfer in nitrogen is rather inefficient, a thousand or more collisions are needed for the gas to thermalize. This means that 5 cm beyond the Mach disc the gas is likely to be below the ambient temperature of the chamber (bear in mind that the gas flow is directed toward the detection region and that molecules will be moving at approximately 500 m s^{-1}). If secondary Mach shock structures are present, the situation might be worse than this. Brune and collaborators (Stevens et al. 1994 and references therein) have estimated a jet temperature ~ 50 K below ambient, 11 cm beyond the nozzle. The rotational temperature of OH at the laser-interaction volume can be verified using fluorescence excitation scans in the (0, 0) band near 308 nm. To model photochemical interference effects this is vital information, since many of the important reactions have strongly temperature-dependent rate coefficients (see section 7). Another potentially important consideration here is that the downstream position of the Mach shock front depends on the ratio $(P_0/P_b)^{1/2}$, so that sampling conditions may change as a function of the ambient pressure. If, as we have argued, the conditions in the downstream subsonic region of the expansion are influenced by the supersonic expansion, day-to-day changes in atmospheric pressure could perturb the results of a FAGE instrument, particularly if the instrument is sampling close to a secondary Mach shock structure.

It is also well known that free-jet expansions can lead to clustering and condensation. Clearly this is undesirable in a FAGE apparatus, as it provides a loss mechanism for OH radicals in the flow and will also result in enhanced Rayleigh, and possibly Mie, scattering. A number of kinetic models for dimer formation in supersonic beams have been developed (Golomb et al. 1970; Gordon et al. 1971; Dorfeld and Hutson 1973; Knuth 1977). However, the kinetics are complex. Miller (1988) suggests some semiempirical rules for assessing the probability of dimer and cluster formation. Dimers are likely to be present at significant concentrations ($\sim 1\%$) if the dimensionless parameter D^* exceeds 0.1, where

$$D^* = \frac{P_0 \sigma^3}{\epsilon} \left(\frac{d}{\sigma}\right)^{0.4} \left(\frac{T_0 k}{\epsilon}\right)^{-2.4}. \qquad (2)$$

and in which σ, ϵ are Lennard–Jones parameters describing the range and depth, respectively, of the intermolecular potential. Similarly trimers, and larger clusters, are present if the parameter C^* exceeds about 15, where

$$C^* = \frac{P_0 \sigma^3}{\epsilon} \left(\frac{d}{\sigma}\right)^{0.88} \left(\frac{T_0 k}{\epsilon}\right)^{-2.3}. \qquad (3)$$

While these expressions are strictly applicable to a monatomic gas, they do provide some sort of criterion for assessing the likely importance of dimer and cluster formation in the FAGE expansion. Experimental data (Beijerinck and Verster 1981) on N_2 are broadly in agreement with these expressions, although it appears that somewhat larger values of C^* and D^* are required. For a typical apparatus, $d = 0.1$ cm, and taking σ for N_2 to be 368 pm and $\epsilon/k = 91.5$ K, we find on substituting into Eqs. (2) and (3) that $D^* = 0.09$ and $C^* = 120$. This suggests that dimeric species will condense to form large clusters and that they are likely to be formed in the expansion at significant concentrations. The model may not be altogether applicable, however, as it assumes that the expansion attains close-to-terminal velocity (see below).

Our apparatus has been designed specifically to permit us to investigate the importance of these potential problems, in that we can control the distance between the nozzle and the laser-interaction region. We intend to characterize the expansion by measuring 1D concentration and temperature gradients along the flow. With our instrument it should be possible to probe both the supersonic and subsonic regions of the expansion. It will be important to investigate the effects of changing the nozzle diameter, since, as we have noted, this defines the characteristic length in axially symmetric free jets. Although there is extensive experimental ev-

idence that shows that for different aperture sizes but otherwise identical source conditions the same beam conditions occur downstream of the nozzle at the same number of nozzle diameters [e.g., Eq. (1)], the terminal beam velocity is almost independent of the nozzle diameter. Thus expansions from smaller nozzles make the transition from continuum to free-molecular flow faster than expansions from larger apertures. In consequence, condensation effects depend fairly strongly on the nozzle diameter. It will also be useful to investigate the possibility of using a slit nozzle, since in 2D free jets the gas density and temperature fall much less rapidly than for an axially symmetric nozzle with the same stagnation pressure and aperture cross section (Kappes and Leutwyler 1988). A potential advantage of a slit nozzle is that the resulting beam is nominally wedge shaped, which offers the possibility of a long *single path* interaction region and which would minimize the generation of secondary OH. It will also be interesting to investigate the possibility of a FAGE system in which the supersonic region is probed since here the flow can be made to be essentially collision free. In this region photochemical interference will be minimal. Furthermore the rotational temperature of the hydroxyl radicals will be low, which enhances the fractional population in the low-lying rotational states. The number density in the beam will also be higher in this region ($n \propto x^{-2}$). We have mentioned already, though, that clustering is a potential problem with the FAGE technique in this region of the expansion. However, following the work of Heaven and collaborators (Heaven 1992), who have investigated the structure and dynamics of OH rare gas clusters, it might be possible to observe OH-N$_2$ spectroscopically in artificially OH-enhanced samples and so assess the degree of clustering directly.

4. Computational fluid dynamics of the jet expansion

The aim of performing computational fluid dynamics (CFD) calculations on the expansion of the ambient air as it passes through the nozzle into the gas beam is to fully describe the spatial variation in temperature, species concentration, and velocities along the beam. Equipped with this model, the experimental apparatus can be designed with the optimum geometry for gas and laser beams to maximize the fluorescence signal from a given sample of ambient OH. In practice CFD calculations need to be refined using experimental data. The cylindrical symmetry inherent in the problem reduces the three-dimensional problem to one involving x and r only, but the boundary conditions are less constrained (slit nozzles will be more difficult unless treated as being infinitely long). Clearly, the modeling needs to account for complex flow phenomena, such as compressible effects, supersonic regions, discontinuity across shock fronts, a complete set of chemical reac-

tions, etc. In particular, an accurate representation of the shock discs is needed. This will not be an easy task. However, the problem may be formulated using multicomponent approximate Riemann solvers (Roe 1981) for the evaluation of convective terms and a standard finite element formulation of the diffusive terms. The addition of an adaptive mesh refinement procedure can improve the spatial resolution by locally dividing elements in regions of high sensitivity, such as across the Mach disc (Flaherty et al. 1989).

The fundamental equation determining the evolution of the velocity field of a viscous, Newtonian fluid is the Navier–Stokes equation

$$\rho \frac{d\mathbf{u}}{dt} = \rho\mathbf{F} - \nabla P + \mu\nabla^2\mathbf{u} + \frac{\mu}{3}\nabla(\nabla\cdot\mathbf{u}), \quad (4)$$

where $\mathbf{u}$ is the velocity vector, P the pressure, μ the viscosity, and $\mathbf{F}$ the body force vector per unit mass. Equation (4) links the rate of momentum "convection" (and therefore velocity) via a "source" term, $-\nabla P$, and a "diffusion" term, $\mu\nabla^2\mathbf{u}$. Similar equations can be derived for the convection rates of matter (i.e., species concentration profiles) and energy (temperature profiles).

Under the steady-state conditions of the FAGE expansion, where the characteristics of the jet remain invariant with time, simpler equations can be written for conservation of mass, momentum, and energy along any of the streamlines of the flow. If the flow is taken as compressible and isentropic, and viscosity and heat conduction terms are neglected, then, in the steady state, these equations may be written as
mass:

$$\nabla\cdot(\rho\mathbf{u}) = 0; \quad (5)$$

momentum:

$$\rho\mathbf{u}\cdot\nabla\mathbf{u} = \rho\mathbf{F} - \nabla P; \quad (6)$$

energy:

$$\mathbf{u}\cdot\nabla H_0 = 0. \quad (7)$$

The equation of state is

$$P = \rho R'T, \quad (8)$$

where R' is the specific gas constant and the thermal equation of state is

$$dH = C_p dT. \quad (9)$$

For an ideal gas the local speed of sound is given by

$$a = \sqrt{\gamma R'T} = \sqrt{\frac{\gamma P}{\rho}} \quad (10)$$

with $\gamma = C_p/C_v$, and substitution enables the main physical properties of the expansion P, ρ, n, and T to

be expressed in terms of the stagnation properties P_0, ρ_0, n_0, and T_0 as functions of only γ and Mach number.

These partial differential equations (PDEs) are elliptic for subsonic flow and hyperbolic for supersonic flows and are readily transformed into the cylindrical coordinate geometry. When the nozzle is short and the flow rate high, viscous effects within the thin boundary layer at the nozzle wall make only small contributions and can be dealt with using a discharge coefficient, C_d, that relates the effective flow source area to the geometric source area.

The two-dimensional hyperbolic PDEs relating to axisymmetric supersonic flow must be solved numerically. In the finite-difference method (Ware and Berzins 1992) the coordinate space is divided into N strips in each direction forming a finite-difference mesh containing $(N - 1)^2$ interior modes. An initial solution for the flow field is assumed, and the method of "nonlinear over-relaxation" is used to solve by finite differences the unsteady-state, time-dependent PDEs as they relax to the steady-state solution. This method has the advantage that it is not restricted to isentropic or supersonic flow, but a very large amount of computing time is required, although adaptive gridding can alleviate this to some extent (Flaherty et al. 1989).

An alternative method determines special "characteristic" curves in space along which the component equations of the PDEs can be combined to yield ODEs for direct numerical integration. The characteristic directions can be conveniently defined as parallel and perpendicular to the local streamline. Transformation between Cartesian or cylindrical coordinates to these characteristic coordinates is relatively straightforward, and computer requirements are significantly reduced. Numerical integration of ODEs can be performed by a suitable library software package such as SPRINT (Berzins et al. 1989), which solves by stiff integration. It should be noted that spectral methods of this sort, while useful in subsonic regions, may run into stability problems close to shock fronts.

Much more problematic are nonequilibrium kinetic effects, since these cause significant deviations from the continuum properties. As the gas expands, the collision frequency drops rapidly, and the rates of kinetic processes—such as internal cooling—slow down and finally stop, as the gas flow enters a transition region from continuum to so-called free-molecular flow. In the transition region the velocity distribution deviates significantly from that of continuum flow. Collisions with background molecules attenuate the beam and rethermalize it. The quantitative analysis of the noncontinuum regime is not straightforward (Miller 1988). One approximation that has proved quite successful is the so-called quitting surface model in which the expansion is divided into two regimes: a continuum isentropic region, followed by a free-molecular, collisionless, region in which the beam "temperature" is frozen. In practice the transition region is quite broad, so the

model is only approximate. It should be possible to model the effects of collisions with background gas molecules downstream of the quitting surface using molecular dynamics or Monte Carlo simulation techniques. These have been previously applied to study nucleation kinetics in beams (Cameron and Harland 1993b; Cameron and Harland 1993a; Lippmann and Schieve 1990; Lippmann et al. 1984).

The transition to free-molecular flow can be estimated as the distance at which the continuum expansion reaches its terminal Mach number $M_\infty = \sqrt{2/\gamma}\,S_\infty$, where S_∞ is the terminal speed ratio given by

$$S_\infty = A\left[\sqrt{2}n_0d\left(\frac{53C_6}{kT_0}\right)^{1/3}\right]^B, \qquad (11)$$

in which A and B are tabulated parameters depending on γ and C_6 is usually expressed in terms of the Lennard–Jones parameters as $4\epsilon\sigma^6$. For an expansion of N_2 through a 1-mm diameter nozzle at atmospheric pressure, we calculate that M_∞ is approximately 30. This value places the quitting surface 190 nozzle diameters downstream of the aperture, beyond the position of the first Mach disc, and indicates that under these conditions continuum flow conditions are likely to be preserved for some distance into the chamber, exhibiting secondary shock structures. Indeed it is doubtful that the flow ever enters the collisionless regime. For "harder" expansions this will not necessarily be the case. Also note that since the transition region is in fact broad, this does not rule out the influence of nonequilibrium effects in current FAGE experiments.

5. The use of rovibrationally excited states for the determination of laser-generated OH

The room temperature absorption cross section of O_3 at 308 nm is only 4% that at 282 nm, and the dissociation quantum yield for production of $O(^1D)$ is 18% smaller (Finlayson-Pitts and Pitts 1986), resulting in a factor of 29 less $O(^1D)$ for the same laser power and pulse duration. In addition, the absorption cross section of OH in the (0, 0) band at 308 nm is ~4 larger than that of the (1, 0) band at 282 nm (Crosley and Chidsey 1981), resulting in an improvement in the sensitivity for OH detection. Despite this and the fact that the rate of reaction between $O(^1D)$ and H_2O to generate OH is slower at reduced pressure, the fraction of the LIF signal from laser-generated OH needs to be assessed directly, particularly for field measurements in polluted environments.

Using an O_3 concentration of 50 ppb, an absorption cross section for O_3 at 308 nm of 1.4×10^{-19} cm^2, a quantum yield for the production of $O(^1D)$ of 0.8 (Finlayson-Pitts and Pitts 1986), and a 5-mm diameter laser beam with pulse energy of 10 μJ, the instantaneous $O(^1D)$ concentration in the FAGE chamber at 2 Torr

total pressure is $\sim 3 \times 10^4$ atoms cm^{-3}. The calculation does not take into account the temporal shape of the laser pulse, but this will be explicitly included in the time-dependent photochemical model described in section 7. The two major pathways for reaction of O(^{1}D) are

$$O(^1D) + M \rightarrow O(^3P)$$
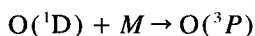
$$k = 2.9 \times 10^{-11} \text{ cm}^3 \text{ molecule}^{-1} \text{ s}^{-1} \quad (12)$$

and

$$O(^1D) + H_2O \rightarrow 2OH$$
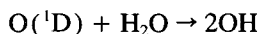
$$k = 2.2 \times 10^{-10} \text{ cm}^3 \text{ molecule}^{-1} \text{ s}^{-1} \quad (13)$$

[kinetic data taken from DeMore et al. (1992)].

Only OH generated in this manner *during the laser pulse* can absorb a further photon at 308 nm and contribute toward the observed LIF signal. Assuming 50% relative humidity at 20°C in the FAGE chamber at 2 Torr (26 m Torr H$_2$O), the concentration of OH formed in Eq. (13) after 25 ns (approximately the laser pulse duration) is $\sim 2.5 \times 10^2$ molecules cm^{-3}.

For an ambient [OH] = 1×10^6 molecules cm^{-3} before expansion, the laser-generated OH in the FAGE chamber at the end of the laser pulse is $\sim 10\%$ of the ambient value. Of course, the majority of the photochemical OH is formed after the laser pulse [approximate OH rise time from reaction (13) is 0.5 μs], and hence it is vitally important that the gas in the laser-interaction volume be completely removed by pumping before the next laser pulse (see section 2).

The above treatment does not take into account the nonstatistical outcome of the reaction between O(^{1}D) and water. Indeed during the laser pulse, the nascent rovibrational distribution of the OH product will remain largely intact. It was first suggested by Smith and Crosley (1990) that the reaction dynamics of this reaction be utilized to assess the degree of photochemical interference. The energy disposal into the internal degrees of freedom of the OH product is summarized in Table 1. Two types of OH product were identified. One corresponds to the "new" O–H bond formed when O(^{1}D) attacks a hydrogen atom in water and is formed with approximately equal populations in $v'' = 0$–2 and extremely high degrees of rotational excitation. The other is the "old" O–H bond that remains essentially unchanged in the reaction and is formed predominantly in $v'' = 0$, although again with considerable rotational excitation (Sauder et al. 1992).

Any signal following excitation of a high rotational level in $v'' = 0$ (the population of ambient OH is negligible above $N'' = 7$) or *any* rotational state in $v'' = 1$ must originate from laser-generated OH and, hence, could form the basis of a method to obtain the relative concentrations of ambient OH to that of laser-generated interference. Ideally, it would be desirable to scan the excitation laser and measure an effective OH popula-

TABLE 1. Energy disposal in the OH products from the reaction $^{16}O(^1D) + H_2^{18}O \rightarrow {^{16}OH} + {^{18}OH}$.[a] The data are taken from Sauder et al. (1992).

Parameter	new ^{16}OH			old ^{18}OH	
	$v = 0$	$v = 1$	$v = 2$	$v = 0$	$v = 1$
$P(v)$[b]	0.39	0.29	[0.3][f]	0.94	0.06
$\langle E_R \rangle$/cm^{-1} [c]	3440	2780	[1600][f]	1920	1610
f_R[d]	0.28	0.32	[0.3][f]	[0.21][f]	
$\langle E_{KE} \rangle$/cm^{-1} [c]		4280		2840	
T_{rot}[g]	19 500	4600	—	4200	2400

[a] ^{16}O(^{1}D) generated from 266-nm photolysis of ^{16}O$_3$.
[b] Relative vibrational population normalized such that $\Sigma_{v=0}^{v=1} P(v)$ = 1 for ^{18}OH.
[c] Average energy distribution averaged over fine-structure states.
[d] Fraction of energy appearing as rotational energy in the fragment assuming that all ^{16}OH fragments are paired with ^{18}OH ($v = 0$) cofragments.
[e] Kinetic energy of fragment averaged over rotational and vibrational states.
[f] Not directly measured.
[g] Rotational "temperature." At low J, rotational temperatures of 400–600 K are observed. Data taken from Cleveland and Wiesenfeld (1992).

tion distribution, but the low signal levels may cause data collection times to be prohibitively long. A more straightforward method is to rapidly scan the laser between two discrete wavelengths, λ_1 and λ_2, exciting from two rotational states labeled A and B, respectively. State A is chosen to have considerable ambient population, with the signal S_A given by

$$S_A = \beta N_A L_A \Phi_A B_A, \quad (14)$$

where β is an experimental proportionality constant—containing factors for the fluorescence collection efficiency, transmission of the optical components, PMT quantum yield, differences in laser and Doppler linewidth, etc.—and is assumed to be constant over the wavelength range between λ_1 and λ_2; N_A is the total number density of molecules in quantum state A; L_A is the laser power at λ_1 (LIF is excited in the linear regime); Φ_A is the fluorescence quantum yield of the excited state following absorption at λ_1, with a correction made for any polarization of the fluorescence (Doherty and Crosley 1984); and B_A is the rotational linestrength function.

The OH number density assay consists of two contributions:

$$N_A = (N_{\text{Amb}} f_A) + (N_{\text{Phot}} P_A), \quad (15)$$

where N_{Amb} is the total number density of ambient OH molecules, f_A is the Boltzmann fraction of these in state A (including the degeneracy), N_{Phot} is the total number density of laser-generated OH, and P_A is the fractional population in state A as measured from energy disposal studies of reaction (13) (Sauder et al. 1992; Cleveland and Wiesenfeld 1992).

For state B, similar equations apply, and if B is chosen such that $f_A \sim 0$, it can be shown that

$$\frac{N_{Phot}}{N_{Amb}} = \frac{f_A \Phi_A S_B}{P_B \Phi_B S_A - P_A \Phi_A S_B}. \quad (16)$$

It is assumed that the laser power and the contribution to the signal from scattered light and fluorescence from other molecules is the same at both wavelengths. Once the ratio N_{Phot}/N_{Amb} is determined, the measured total OH concentration can be corrected for photochemical interference.

Previously, laser-generated OH was determined by chemical modulation, whereby addition of isobutane or C_3F_6 removes the ambient OH before the laser-interaction region, and hence, only laser-generated OH is detected. However, isobutane reacts with $O(^1D)$ to form OH, and any modifer can quench OH LIF when added in quantities sufficient to remove the ambient OH. The proposed method is nonintrusive, eliminating these problems, but complications may arise from the state-specific nature of the quantum yield for fluorescence, defined for the excited state $|i\rangle$ as

$$\Phi_i = \frac{A_i}{A_i + Q_i + P_i}, \quad (17)$$

where A, Q, and P are the state-specific radiative, quenching, and predissociation rates, respectively. The radiative rates are well known for OH in a large number of rotational states within the $A\,^2\Sigma^+$ rovibrational manifold (Chidsey and Crosley 1980), and the predissociation rate can be neglected for $v' = 0$. The quenching rate can be expressed as a series expansion:

$$Q_i = \sum_i C_q k_{i,q}(T), \quad (18)$$

where C_q is the number density of collider q that quenches OH in state $|i\rangle$ to the ground electronic state with a rate constant $k_{i,q}(T)$. Both discharge flow studies (Copeland et al. 1985; Wysong et al. 1990; Burris et al. 1991) and flame studies (Jeffries et al. 1988; Cattolica and Mataga 1991) have measured $k_{i,q}$ for a large number of collider species and over a wide range of excited states $\{|i\rangle\}$ (mainly in $v' = 0$, 1 from N' $= 0 \rightarrow 5$). The quenching-rate constant was found to be strongly dependent upon the value of the rotational quantum number N' (Copeland et al. 1985) and the temperature T (Jeffries et al. 1988; Copeland and Crosley 1986), decreasing with both N' and T. Therefore, it is possible to calculate Q_i if the gas composition is known and, hence, Φ_i from Eq. (17). This then enables the N_{Phot}/N_{Amb} ratio to be found. Although the quenching rate has been measured at high temperatures in flames (Jeffries et al. 1988), there are no quenching data for high rotational levels at room temperature.

If state B is chosen to be in $v'' = 1$ (20% of the OH formed in reaction (13) is in $v'' = 1$), excitation to v' $= 1$ via the (1, 1) band near 314 nm will be followed

by rapid, vibrational energy transfer (VET) into v' $= 0$, the rate of which is comparable to the quenching rate from $v' = 1$ and is rotational-level dependent (Copeland et al. 1988). The VET must be taken into account to calculate the value of Φ_B. Collisional repopulation of the laser-pumped level A or B during the laser pulse is only important if the OH transition is close to optical saturation, and so although these energy transfer rates vary with N'', this dependence need not be taken into account at the laser energies used in this experiment.

Clearly it is hoped that the degree of laser-generated OH interference is small, as is suggested by the results of others employing FAGE at 308 nm (Chan et al. 1990; Crosley 1992; Stevens et al. 1994, and references therein; Hofzumahaus and Holland 1993). However, a nonintrusive in situ method to assess the interference is still desirable, particularly during field measurements in polluted environments. Initially, calibrated concentrations of O_3 and water above ambient levels will be introduced to the nozzle flow, to markedly increase the N_{Phot}/N_{Amb} ratio and validate the above method. Repeating the experiment under ambient conditions will then allow, for the first time, the ratio to be measured directly. In addition, other potential contributions to the fluorescence signal at 308 nm—such as OH production from photolysis of pollutants, for example, HNO_3, HONO or H_2O_2 (OH is formed in highly excited rovibrational states)—can be studied in the same manner. The background fluorescence signal from non-OH sources will be measured by scanning the laser away from an OH transition. A reference cell, in which OH is generated at much higher than ambient concentrations, will enable the laser to be accurately tuned either on- or off-resonance with a transition of OH.

The translationally "hot" OH generated in reaction (13) will have a Doppler-broadened absorption linewidth of ~ 0.4 cm^{-1}, considerably larger than either the ambient OH Doppler width (~ 0.1 cm^{-1}) or the frequency-doubled etalon-narrowed laser line width (~ 0.06 cm^{-1}). Short scans of the laser wavelength from line center to the wings may then allow the contribution from laser-generated OH to be found, although relaxation of the nascent OH distribution will proceed at a gas kinetic rate (Gericke and Comes 1982) and must be taken into account.

The excitation of OH via the (1, 0) band at 282 nm is known to create a large concentration of photochemical OH (Smith and Crosley 1990, and references therein), and because of problems in quantifying its contribution to the overall LIF signal, this scheme has all but been abandoned in the quest for accurate measurements of tropospheric OH concentrations. However, excitation via the (1, 0) band, and selective collection of fluorescence in the (0, 0) and (1, 1) bands at 308 nm, offers a significant advantage: the PMT is insensitive to scattered light at the laser wavelength and need not be gated. Gating has been shown to introduce

an after-pulse signal that leads to increased noise levels (Hofzumahaus and Holland 1993). The use of high rotational states would offer a nonintrusive and quantitative method to measure the N_{Phot}/N_{Amb} ratio.

6. Calibration of the LIF signal to yield OH concentrations

The LIF signal does not yield directly the OH concentration, and perhaps the largest error during the FAGE experiment is incurred in the calibration of the LIF signal. There are two key problems with calibration: 1) producing a known concentration close to that of the ambient value and under similar experimental conditions and 2) ascertaining the fraction of the OH that is lost between its production and the laser excitation volume.

Very little is known about the OH losses, with studies largely restricted to empirical observations, for example, those that show that the signal is relatively insensitive to the material used to fabricate or coat the nozzle (Stevens et al. 1994 and references therein), although recent results from the Jülich group indicate problems arising from the coating of the FAGE chamber itself (A. Hofzumahaus 1994, personal communication). In addition, the fluorescence quantum yield for a particular excited state of OH is different for ambient and calibration conditions due to differing chemical environments, and hence it is unlikely that the loss of calibrated OH is the same as for ambient OH. The photochemical model described in section 7 will incorporate such issues and allow corrections to be made.

We intend to use several of the calibration methods that are common to existing FAGE systems (Stevens et al. 1994 and references therein; Hofzumahaus and Holland 1993; Chan et al. 1990); these are described as 1)–3) below.

1) A well-established method to generate a known concentration of OH uses a fast titration reaction in a discharge flow system:

$$H + NO_2 \rightarrow NO + OH \qquad (19)$$
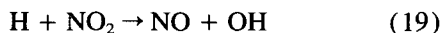
$$k = 1.98 \times 10^{-10} \text{ cm}^3 \text{ molecule}^{-1} \text{ s}^{-1}.$$

Hydrogen atoms are generated in a microwave discharge, in excess of an accurately known flow of NO_2, and quantitative conversion to OH occurs. The method has an upper pressure limit of about 10 torr and hence is not suitable for calibration at atmospheric pressure using the FAGE nozzle. If the nozzle is replaced by a flow tube for calibration purposes, an accurately known amount of OH can be generated at the laser-interaction volume and at the *same* total pressure as in the monitoring experiment. This method has a lower limit of [OH], $\sim 10^8$ molecules cm^{-3}, with an uncertainity of $\sim 30\%$ (Stevens et al. 1994 and references therein), and again the photochemical model will be used to optimize conditions for the production of OH and to minimize the homogeneous loss of OH through recombination reactions, for example, OH + NO → HONO. Although straightforward to implement, the calibration will yield an underestimate of the ambient OH concentration, due to losses that must occur when the nozzle is in position.

2) Calibration at atmospheric pressure (i.e., generating OH outside the FAGE chamber followed by nozzle expansion) is performed using a photochemical reaction with a unity quantum yield for production of OH. We will use the photolysis of water at 184.9 nm,

$$H_2O + h\nu \rightarrow OH + H, \qquad (20)$$

to generate known concentrations of OH given by

$$[OH] = [H_2O]\sigma\phi t, \qquad (21)$$

where σ is the absorption cross section of H_2O at 184.9 nm (5.5×10^{-20} cm^2), ϕ is the photon flux at 184.9 nm from a calibrated Hg lamp, and t is the photolysis time. Generation of OH concentrations at the 10^7–10^8 molecule cm^{-3} level are reported (Stevens et al. 1994 and references therein), but a major difficulty is the accurate determination of [H_2O] for which a cold mirror hygrometer is used (Stevens et al. 1994 and references therein). The concentration [H_2O] is also required to calculate the fluorescence quantum yield of OH in the FAGE chamber. Gases must be scrupulously cleaned to prevent impurities from reacting with OH both before and in the nozzle region. If a small amount of O_2 is added to the system, H atoms formed in reaction (20) are converted to HO_2, and in the absence of impurities that remove OH, the [HO_2]/[HO] ratio should be 1 or less. This ratio can be measured by converting the HO_2 to OH through injection of NO at the nozzle and detecting the total OH LIF signal. A ratio of [HO_2]:[OH] > 1 indicates the removal of some OH via reaction with impurities. The uncertainty with this calibration is stated as 50% [Stevens et al. (1994), and references therein] and mainly due to nonuniformity of the gas flow and the UV flux.

Method 2) is associated with large errors once the [H_2O] becomes difficult to measure at low concentrations. An alternative method to obtain [H_2O] is through its appearance in the expression for the fluorescence lifetime of the $A^2\Sigma^+$ state of OH:

$$\tau^{-1} = A + Q, \qquad (22)$$

with the quenching contribution given by Eq. (18) above. For an atmosphere consisting of a dilute mixture of H_2O in N_2, Q is given by

$$Q = k_q[H_2O] + k_{q'}[N_2], \qquad (23)$$

with k_q and $k_{q'}$ being the quenching rate constants with H_2O and N_2, respectively. At 300 K and for $N' = 2$, $k_q = 6.8 \times 10^{-10}$ (Wysong et al. 1990) and $k_{q'} = 3.1 \times 10^{-11}$ cm^3·molecule^{-1} s^{-1} (4.8×10^{-11} cm^3 molecule^{-1} s^{-1} at 232 K) (Copeland and Crosley 1986).

For 50% relative humidity at 300 K and expanding into 2 Torr, $Q = 2.6 \times 10^6$ s^{-1} (~20% of this from H$_2$O), and taking $A = 10^6$ s^{-1}, τ is ~0.3 μs. Halving the water concentration will change the lifetime by ~7%. It is planned to use a multichannel scaler (5-ns resolution) to measure the fluorescence lifetime and, hence, [H$_2$O]. The z-translator will allow such a measurement at a number of points inside the FAGE chamber and used to validate the photochemical model. Comparison of the calibration factor (signal/[OH] at a given laser power) measured for methods 1) and 2) above ought to give information on the losses incurred in the nozzle. However, correcting for the differing quenching environments is not straightforward and will be aided by direct lifetime measurements.

Hydrogen atoms can be detected with good sensitivity by absorption at the Lyman-α wavelength (121.5 nm). Using an integrated absorption cross section at 298 K of 3.6×10^{-13} cm^2, the Beer–Lambert law predicts ~0.5% absorption for a pathlength of 5 cm and [H] = 2.5×10^9 atoms cm^{-3}.

The reaction

$$O(^1D) + H_2 \rightarrow OH + H \qquad (24)$$
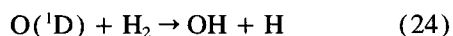
$$k = 1.10 \times 10^{-10} \text{ cm}^3 \text{ mol}^{-1} \text{ s}^{-1} \qquad (25)$$

generates OH and H in the ratio 1:1, with $O(^1D)$ generated from the 253.7-nm photolysis of O$_3$ using a calibrated Hg lamp. Therefore, a direct absorption measurement of [H], although difficult, might be feasible to calibrate the OH LIF signal in the FAGE chamber. It will be extremely important to rigorously exclude any traces of water that will absorb radiation at 121.5 nm, and the spectral output of the resonance lamp must be well characterized. A chopper will modulate the 121.5-nm radiation, allowing phase-sensitive detection to improve the signal to noise ratio of the absorption measurement. In addition, laser photolysis of a known concentration of O$_3$ in the presence of excess water vapor can be used to generate a pulsed, known concentration of OH over the range 10^9–10^{11} cm^{-3}.

In order to measure the concentration of HO$_2$, NO is added to the gas flow to convert it to OH, with subsequent detection by LIF. The conversion efficiency will not be 100% and therefore must be measured. It is intended to use the method of Stevens et al. (1994 and references therein) for this purpose. OH is generated using photolysis of H$_2$O as described above and quantitatively converted to HO$_2$ via the reactions

$$OH + CO \rightarrow H + CO_2 \qquad (26)$$

$$H + O_2 \rightarrow HO_2. \qquad (27)$$
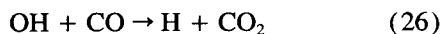
The HO$_2$ is converted back to OH by the addition of NO after the nozzle, and assuming that the losses in the nozzle expansion are identical for OH and HO$_2$, the OH LIF signal should remain unchanged irrespective of whether CO is present or not. Any reduction in OH

signal on addition of CO directly reflects the conversion efficiency of HO$_2$ to OH. The photochemical model will be used to predict the optimum experimental conditions for this conversion, and comparison with experiment will provide another validation. The addition of too much NO will deplete OH via the addition reaction to form nitrous acid.

7. Photochemical models

A detailed photochemical model for a hydroxyl radical detection system based on LIF has been developed by Smith and Crosley (1990). Their analysis referred to the off-resonance (282-nm excitation, 308-nm detection) FAGE technique developed by Hard et al. (1984, 1986). They quantitatively demonstrated the origins of ozone interference and saturation effects and suggested improvements in the experimental methodology.

Smith and Crosley established the principles of photochemical modeling for OH detection that will be followed, and extended where necessary, in our own modeling studies. The aims are to construct a computer model that is based on experimental reaction and energy transfer parameters and to employ that model to determine optimal operational conditions. It would also be advantageous if the model were, or could be made, sufficiently compact and computationally efficient so that it could be used in the on-line analysis of field data.

The central technique proposed in section 5 involves monitoring either high rotational states in $v'' = 0$ or any rotational states in $v'' = 1$ to correct the low $v'' = 0$, N'' states for photochemical interference. The following processes need to be incorporated in the model; most have already been discussed in section 5:

1) Photolysis of ozone at 308 nm to generate $O(^1D)$ and $O(^3P)$. Photolysis of H$_2$O$_2$ will also need to be included.

2) Production of OH $X^2\Pi(v'', N'')$ by reaction of $O(^1D)$ with H$_2$O. It is proposed not to include chemical modulation in the detection scheme, so that generation of OH from O^1D + modulator is not required. If necessary, such a process could be readily incorporated. Reaction of $O(^1D)$ with ambient nonmethane hydrocarbons at ppb levels or with methane at ppm levels will not be significant.

3) Vibrational and rotational relaxation of OH ($X^2\Pi$).

4) Absorption, stimulated, and spontaneous emission of OH.

5) Quenching and rotational relaxation of $A^2\Sigma^+$ ($v = 0, 1$) and vibrational relaxation of $A^2\Sigma^+$ ($v = 1$).

Some of the data needed to construct and implement this model at operational temperatures are not available in the literature. Experiments designed to provide these data are discussed below in section 8.

The computer code SPRINT will be employed for numerical integration (Berzins et al. 1989). SPRINT is a general purpose package for the numerical solution of coupled sets of time-dependent algebraic, ordinary and partial differential equations. It contains a number of components, including stiff integrators, enabling the user to tailor the code for a wide variety of problem classes. It is flexible and efficient and allows greater user control, at the expense of programming effort, than does the CHEMKIN (Kee et al. 1989) package used by Smith and Crosley. Several of the problems they encountered (e.g., initial conditions, state-specific thermodynamics, optical pumping rates) can consequently be readily overcome. It will be necessary to incorporate detailed balance explicitly, although this is readily achieved.

In order to model the effects of photochemically generated OH ($X^2\Pi_i$) Smith and Crosley (1990) lumped the states into components of the ambient and hot photolytic distributions that were assigned a temperature. The laser-coupled states in both OH ($X^2\Pi_i$) and OH ($A^2\Sigma^+$) were explicitly described. They tested the procedure at 300 K by comparing partial and Boltzmann populations. While this approach is efficient and probably realistic, it does make implicit assumptions about the nature of the population distributions that are not explicitly justified. We are employing an alternative approach that starts from a complete description of the system and then employs objective lumping procedures to generate an efficient model. The model consists of a set of coupled ordinary differential equations (ODEs) describing the time dependence of all the rovibrational states of OH ($A^2\Sigma^+$) and OH ($X^2\Pi_i$), including fine-structure doublets and spin components, and other species for example, O(^{1}D), etc. All the terms in the ODEs are first order or pseudo–first order, which considerably simplifies the analysis. The full model will be integrated for a representative range of experimental conditions, providing measures of "reality" against which reduced and lumped models can be validated.

Lumping represents a powerful technique for reducing the dimensionality of the chemical model. A familiar example, which relies on the existence of widely separated timescales, is the use of the quasi-steady-state approximation (QSSA) (Tomlin et al. 1992), which allows the time derivatives of the fast variables to be set to zero on the slower timescale of the main chemical evolution of the system. This procedure replaces some of the ODEs with algebraic equations and, especially for systems dominated by pseudo-first-order reactions, allows the short-lived species to be described analytically in terms of the longer-lived species.

Lumping relations need not necessarily be formulated on the basis of timescales, and a general analysis of lumping techniques has been carried out in kinetic systems by Li and Rabitz (1989, 1990). The primary aim of lumping techniques is the reduction of a system of ordinary differential equations to a lower dimen-

sional system that represents the essential dynamics of the full equations. The reduction is achieved by the transformation of the original variables to a smaller set of lumped variables via linear or nonlinear functions. In the case of first-order reaction systems this can be through linear combinations of the original ones. The choice of linear combination is based on an eigenvalue–eigenvector analysis of the Jacobian matrix. A subspace of the original eigenvectors can be used to form the lumping matrix defining the transformation to new lumped species. This ensures that the lumped system will contain some of the eigenvalue structure of the original system and, therefore, some of the same dynamics. The choice of subspace is, however, very important and will depend on certain physical aspects of the model and on the behavior that the reduced model should represent. Information about timescales is one criterion that can be used to select an appropriate subspace. The fast subspace relating to large negative eigenvalues can be discarded, giving a lumped set of slow variables that are a good representation of the long time behavior.

The advantage of this approach is that it generates fast and efficient computational procedures to be generated objectively from the full model without a priori assumptions. The Smith and Crosley model employed a lumped mechanism that was derived using chemical and physical intuition. It may turn out that this lumped mechanism is the one generated by the procedures described above. The advantage of employing the proposed methodology, however, is that the approximations are generated objectively, and their accuracy can be assessed quantitatively at each stage.

8. Accompanying kinetic experiments

In order to obtain the fluorescence quantum yield Φ for OH excited at 308 nm to $v' = 0$, both quenching and rotational energy transfer (RET) rates are required at the below ambient temperature of the FAGE expansion. The former vary strongly with rotational level (Copeland et al. 1985), and hence any rotational redistribution following excitation to a single N' level will change the value of Φ and hence impact on the FAGE measurement. Rotational-level-specific quenching rates for OH in $v' = 0$ are well known at room temperature, and there are less extensive data at elevated temperatures (mainly from flame studies) and down to 230 K, using a cooled flow tube (Copeland and Crosley 1986). Measurements of RET rates are more sparse, with data obtained at room temperature only using two methods: 1) high-resolution fluorescence scans following excitation to a specific N' level within $v' = 0$ (Crosley 1991), measured as a function of collider pressure, and 2) temporal resolution of the fluorescence from the initially excited and the collisionally populated rotational levels (Jorg et al. 1990).

Interesting propensities were observed that were qualitatively understood from the nature of the inter-

molecular potential energy surface between $OH(A^2\Sigma)$ and the collider. However, data acquisition times are long, and hence data are available only for a small number of initially excited levels for each collider, and the only atmospheric collider studied was N_2. It is intended to use the high-speed data acquisition capabilities of the Cu dye laser system, coupled with a variable temperature discharge-flow system, to measure the RET rates for N_2, O_2, CO_2, and H_2O at and below ambient temperatures.

At room temperature the thermal population limits the maximum N' level that can be accessed to ~6. To use the method outlined in section 5 to assess photochemical OH, as well as for input to the model, quenching and RET rates for high N' are required. A photolytic source of OH will be employed, using, for example, 193-nm excimer-laser photolysis of HNO_3, to generate OH in highly rotationally excited N'' levels in $v'' = 0$ or 1, which are then excited to $N' = N'' \pm m$ ($m = 0, 1, 2$) with a tunable dye laser.

A resurrection of FAGE based on excitation of OH at 282 nm requires knowledge of the quenching rates of $v' = 1$ and vibrational energy transfer (VET) rates into $v' = 0$. Low-resolution fluorescence scans enable emission from $v' = 1$ and $v' = 0$ to be isolated, and experiments performed as a function of collider gas pressure to yield the VET rates (Copeland et al. 1988). For some colliders these were found to be similar to quenching and RET rates, and hence the rotational distribution in $v' = 0$ following VET is far from thermal (Williams and Crosley 1995), affecting the fluorescence quantum yield. No data have been published at below ambient temperatures, and measurements of VET and quenching rates at low temperature are planned.

REFERENCES

Beijerinck, H. C. W., and N. F. Verster, 1981: Absolute intensities and perpendicular temperatures of supersonic beams of polyatomic gases. *Physica*, **111C**, 327–352.

Berzins, M., R. M. Furzeland, and P. M. Dew, 1989: Developing software for time-dependent problems using the method of lines and differential algebraic integrators. *J. Appl. Numer. Math.*, **5**, 375–397.

Bradshaw, J. D., M. O. Rodgers, and D. D. Davis, 1984: Sequential two-photon laser-induced fluorescence: A new technique for detecting hydroxyl radicals. *Appl. Opt.*, **23**, 2134–2140.

Burris, J., J. Butler, T. McGee, and W. Heaps, 1991: Quenching and rotational transfer rates in the $v' = 0$ manifold of OH ($A^2\Sigma^+$). *Chem. Phys.*, **151**, 233–238.

Cameron, B. R., and P. W. Harland, 1993a: Application of the thermal conduction model to rotational relaxation. *J. Chem. Soc. Faraday Trans.*, **89**, 1903–1907.

——, and ——, 1993b: Monte-Carlo calculation of rotational relaxation in small molecules. *J. Chem. Soc. Faraday. Trans.*, **89**, 3517–3525.

Campargue, R., 1984: Progress in overexpanded supersonic jets and skimmed molecular beams in free-jet zones of silence. *J. Phys. Chem.*, **88**, 4466–4474.

Cattolica, R. J., and T. G. Mataga, 1991: Rotational level dependent quenching of OH $A^2\Sigma^+(v' = 1)$ by collisions with H_2O in a low pressure flame. *Chem. Phys. Letts.*, **182**, 623–631.

Chan, C. Y., T. M. Hard, A. A. Mehrabzadeh, L. A. George, and R. J. O'Brien, 1990: Third-generation FAGE instrument for tropospheric hydroxyl radical measurement. *J. Geophys. Res.*, **95**, 18 569–18 576.

Chidsey, I. L., and D. R. Crosley, 1980: Calculated rotational transition probabilities for the *A-X* system of OH. *J. Quant. Spectrosc. Radiat. Transfer*, **23**, 187–199.

Cleveland, C., and J. R. Wiesenfeld, 1992: Nascent product population distribution in the reaction $^{16}O_2 + H_2^{18}O \rightarrow {}^{16}OH + {}^{18}OH$. *J. Chem. Phys.*, **96**, 248–255.

Copeland, R. A., and D. R. Crosley, 1986: Temperature dependent electronic quenching of OH ($A^2\Sigma^+$, $v' = 0$). *J. Chem. Phys.*, **84**, 3099–3105.

——, M. J. Dyer, and D. R. Crosley, 1985: Rotational level dependent quenching of $A^2\Sigma^+$ OH and OD. *J. Chem. Phys.*, **82**, 4022–4032.

——, M. L. Wise, and D. R. Crosley, 1988: Vibrational energy transfer and quenching of OH ($A^2\Sigma^+$, $v' = 1$). *J. Phys. Chem.*, **92**, 5710–5715.

Crosley, D. R., 1991: Collisional effects in laser detection of tropospheric OH. *Proc. SPIE*, **1433**, 58.

——, 1992: Local measurement of tropospheric HOx. NASA Conf. Publ. 3245, 76 pp.

——, and I. L. Chidsey, 1981: Tables of calculated transition probabilities for the A-X system of OH. U.S. Army Tech. Rep. (BRL) ARBRL-TR-02326, 56 pp.

Davis, D. D., W. Heaps, and T. McGee, 1976: Direct measurements of natural tropospheric levels of OH via an aircraft borne tunable dye laser. *Geophys. Res. Lett.*, **3**, 331–333.

DeMore, W. B., and Coauthors, 1992: Chemical kinetics and photochemical data for use in stratospheric modelling. Evaluation number 10. NASA/JPL Publ. 92–20, 241 pp.

Doherty, P. M., and D. R. Crosley, 1984: Polarisation of laser-induced fluorescence in OH in an atmospheric pressure flame. *Appl. Opt.*, **23**, 713–721.

Dorfeld, W. G., and J. B. Hutson, 1973: Condensation in CO_2 free jet expanisons. Part I: Formation. *J. Chem. Phys.*, **59**, 1253–1260.

Finlayson-Pitts, B. J., and J. N. Pitts, 1986: *Atmospheric Chemistry. Fundamentals and Experimental Techniques.* J. Wiley and Sons, 1098 pp.

Flaherty, J. E., P. J. Paslow, M. S. Shephard, and J. D. Vasilakis, Eds., 1989: *Adaptive Methods for Partial Differential Equations.* Society for Industrial Applied Mathematics.

Gericke, K. H., and F. J. Comes, 1982: Energy partitioning in the reaction $O(^1D) + H_2O \rightarrow OH + OH$. V, Rotational relaxation of OH ($X^2\Pi$, v'', J''). *Chem. Phys.*, **65**, 113–121.

Golomb, D., R. Good, and R. Brown, 1970: Dimers and clusters in free jets of Argon and Nitric Oxide. *J. Chem. Phys.*, **52**, 1545–1551.

Gordon, R. J., Y. T. Lee, and D. R. Herschbach, 1971: Supersonic molecular beams of alkali dimers. *J. Chem. Phys.*, **54**, 2393–2409.

Hard, T. M., R. J. O'Brien, C. Y. Chan, and A. A. Mehrazbzabeh, 1984: Tropospherical free radical determination by FAGE. *Environ. Sci. Technol.*, **18**, 768–777.

——, C. Y. Chan, A. A. Mehrabzadeh, W. H. Pan, and R. J. O'Brien, 1986: Diurnal cycle of tropospheric OH. *Nature*, **322**, 617–620.

——, C. Y. Chan, A. A. Mehrazbzabeh, and R. J. O'Brien, 1992a: Diurnal HO_2 cycles at clean air and urban sites. *J. Geophys. Res.,* **97,** 9785–9794.

——, A. A. Mehrazbzabeh, C. Y. Chan, and R. J. O'Brien, 1992b: FAGE measurements of tropospheric OH measurements and model of interferences. *J. Geophys. Res.,* **97,** 9795–9817.

Heaven, M. C., 1992: Spectroscopy and dynamics of open-shell Van der Waals molecules. *Annu. Rev. Phys. Chem.,* **43,** 283–310.

Hofzumahaus, A., and F. Holland, 1993: LIF based detection system for measurements of tropospheric OH using 308 nm excitation at low pressure. *Proc. SPIE,* **1715,** 163–173.

——, H. P. Dorn, and U. Platt, 1990: Tropospheric OH radical measurement techniques: Recent developments. *Physico-Chemical Behaviour of Atmospheric Pollutants. Proc., Fifth European Symp.,* Varese, Italy, European Commission, 103–108 pp.

Jeffries, J. B., K. Kohse-Hoinghaus, G. P. Smith, R. A. Copeland, and D. R. Crosley, 1988: Rotational level dependent quenching of OH $(A^2\Sigma^+)$ at flame temperatures. *Chem. Phys. Letts.,* **152,** 160–166.

Jorg, A., U. Meier, and K. Kohse-Hoinghaus, 1990: Rotational energy transfer in OH $(A^2\Sigma^+, v' = 0)$ — A method for the direct determination of state-to-state transfer coefficients. *J. Chem. Phys.,* **93,** 6453–6462.

Kappes, M., and S. Leutwyler, 1988: Molecular beams of clusters. *Atomic and Molecular Beam Methods,* G. Scoles, Ed., Oxford University Press, 380–415.

Kee, R. J., F. M. Rupley, and J. A. Miller, 1989: Chemkin-II: A FORTRAN chemical kinetics package for the analysis of gasphase chemical kinetics. Sandia National Laboratories Tech. Rep. SAND89-8009B.

Knuth, E. L., 1977: Dimer formation rate coefficients from measurements of terminal dimer concentrations in free-jet expansions. *J. Chem. Phys.,* **66,** 3515–3525.

Li, G., and H. Rabitz, 1989: A general analysis of exact lumping in chemical kinetics. *Chem. Eng. Sci.,* **44,** 1413–1430.

——, and ——, 1990: A general analysis of approximate lumping in chemical kinetics. *Chem. Eng. Sci.,* **45,** 977–1002.

Lippmann, D., and W. C. Schieve, 1990: Time dependence of condensation—A kinetic model. *J. Chem. Phys.,* **92,** 4426–4432.

——, ——, and C. Canestaro, 1984: Clustering time-dependence in molecular dynamics: A kinetic model. *J. Chem. Phys.,* **81,** 4969–4978.

Miller, D. R., 1988: Free jet sources. *Atomic and Molecular Beam Methods,* G. Scoles, Ed., Oxford University Press, 14–53.

Roe, P. L., 1981: Approximate Riemann solvers, parameter vectors, and difference schemes. *J. Comput. Phys.,* **43,** 357–372.

Sauder, D. G., J. C. Stephenson, D. S. King, and M. P. Casassa, 1992: Nascent product states in the photoinitiated reaction of O_3 and H_2O. *J. Chem. Phys.,* **97,** 952–961.

Smith, G. P., and D. R. Crosley, 1990: A photochemical model of ozone interference effects in laser detection of tropospheric OH. *J. Geophys. Res.,* **95,** 16 427–16 442.

Stevens, P. S., J. H. Mather, and W. H. Brune, 1994: Measurement of tropospheric OH and HO_2 by laser-induced fluorescence at low pressure. *J. Geophys. Res.,* **99,** 3543–3557.

Tomlin, A. S., M. J. Pilling, T. Turanyi, J. H. Merkin, and J. Brindley, 1992: Mechanism reduction for the oscillatory oxidation of hydrogen—Sensitivity and quasi-steady-state analysis. *Comb. Flame,* **91,** 107–130.

Wang, C. C., L. I. Davis, C. H. Wu, and S. Japar, 1976: Laser-induced dissociation of ozone and resonance fluorescence of OH in ambient air. *Appl. Phys. Lett.,* **28,** 14–16.

Ware, J., and M. Berzins, 1992: Finite volume techniques for time-dependent fluid-flow problems. *Advances in Comp. Maths.,* R. Vichnevestky, D. Knight, and G. Richter, Eds., IMACS, Rutgers University, p. 794.

Williams, L. R., and D. R. Crosley, 1995: Rotational distribution in $v' = 0$ following vibrational energy transfer from OH $(A^2\Sigma^+, v' = 1)$ at 300 K. *J. Chem. Phys.,* submitted.

Wysong, I. J., J. B. Jeffries, and D. R. Crosley, 1990: Quenching of OH $(A^2\Sigma^+)$ at 300 K by several colliders. *J. Chem. Phys.,* **92,** 5218–5222.